Journal of Engineering Research (Libya)

A HYBRID EXPERIMENTAL-NUMERICAL APPROACH FOR STRUCTURAL HEALTH MONITORING USING SEM AND MEASURED FRF

Khaled M. Ahmida

Department of Mechanical and Industrial Engineering
Faculty of Engineering, University of Tripoli
Email: k.ashouri@uot.edu.ly
Received 17 March 2026; Revised 23 April 2026; Accepted 24 April 2026; Published 12 May 2026.

منهج تجريبي-عددي هجين لمراقبة السلامة الإنشائية باستخدام طريقة العناصر الطيفية ودوال الاستجابة الترددية

خالد محمد احميده العاشوري

قسم الهندسة الميكانيكية والصناعية، كلية الهندسة، جامعة طرابلس، ليبيا

الملخص

حظيت طرق كشف الضرر في الهياكل المعتمدة على الاهتزاز باهتمام كبير نظراً لكونها غير إتلافيه ضمن ما يُعرف بمراقبة الحالة الهيكلية (SHM). تُعد الSHM ضرورية لضمان سلامة وأداء الأنظمة الهندسية، وتكتسب التقنيات غير الإتلافيه المعتمدة على الاهتزازات الميكانيكية قيمة خاصة لأنها تتيح الكشف المبكر عن الضرر. تتطلب العديد من الطرق معلومات حول مصفوفات الصلابة للهيكل وهو ما يصبح صعب الحصول عليه في الهياكل الحقيقية. تقترح هذه الورقة نهجاً حسابياً جديداً لمراقبة الحالة الهيكلية، يعتمد على حساب الطاقات الكامنة من دوال استجابة التردد المقاسة الناتجة عن التشوهات المرنة في الهياكل. تهدف هذه الدراسة إلى تطوير طريقة تحدد موضع الضرر بمقارنة الطاقات الكامنة المحسوبة من دوال الاستجابة للتردد المجمعة عند مجموعة نقاط قبل وبعد حدوث الضرر. تستخدم الطريقة المقترحة صيغ طريقة العنصر الطيفي لهياكل ثلاثية الأبعاد لحساب الطاقات الكامنة من دوال الاستجابة للتردد. تُظهر المحاكاة العددية، بافتراض عدة نسب للضرر، أن التغيرات في الطاقة الكامنة المحسوبة تشير بشكل موثوق إلى حدوث الضرر وتحدد موقعه. استُخدما مؤشّران لتحديد موضع التلف؛ مؤشر عام يعطي قيمة عبر نطاق التردد الكامل؛ ومؤشر يركّز تحديداً على الاستجابات عند ذبذبات الرنين. نجحت المنهجية المقترحة في تحديد أضرار تصل نسبتها إلى 5%، ممثلة بتغير في الخواص الهندسية للهيكل نتيجة حدوث الضرر. استُخدمت دوال خاصة لافتراض ضوضاء غاوسية بيضاء وذلك بإدخال نسبة إشارة-ضوضاء (SNR) مقدارها 25 ديسيبل في دوال الاستجابة لمحاكاة الضوضاء التجريبية. تُعتبر هذه القيمة 25 ديسيبل عادة الحد الأدنى المقبول به. أُظهرت النتائج أن الطريقة بسيطة التطبيق إذ تتطلب فقط قياسات دوال الاستجابة للتردد، وحققت دقة ملحوظة في كشف وتحديد موضع الضرر، مما يدعم تطبيق أوسع لتقنيات قائمة على طريقة العنصر الطيفي في مراقبة الحالة الهيكلية العملية.

الكلمات المفتاحية: الأضرار الانشائية، الطريقة المعتمدة على الاهتزازات، طريقة العناصر الطيفية، انتشار الموجات في الانشاءات، النهج المختلط.

Copyright © 2026 by Faculty of Engineering, University of Tripoli, Libya.
This work is licensed under a Creative Commons Attribution 4.0 International License, which permits unrestricted use, distribution, and reproduction in any medium, provided the original work is properly cited.

ABSTRACT
Vibration-based damage detection methods have gained significant attention due to their non-destructive nature in what is referred to as Structural Health Monitoring (SHM). The SHM is essential for ensuring safety, reliability, and long-term performance of engineered systems; non-destructive vibration-based techniques are particularly valuable because they allow early detection of damage without interrupting service. Many approaches require information about the stiffness matrices of the structure, as in Modal Strain Energy (MSE) method, which becomes somehow difficult to obtain in real structures. This paper proposes a new hybrid computational approach for SHM, based on calculating the potential energies from the measured Frequency Response Functions (FRFs), due to elastic deformations in the structure. This study aims to develop and validate a hybrid, frequency-domain method that identifies and localizes damage by comparing potential energies computed from measured FRFs collected at multiple points before and after the damage. The proposed method uses Spectral Element Method (SEM) formulations for 3D frame waveguides (rod, shaft, and beam) to compute the potential energies from FRFs. Therefore, avoiding the need for explicit stiffness matrices as required by other approaches. Numerical simulations across several damage percentages demonstrate that changes in the computed potential energy reliably indicate damage occurrence and location. Two damage localization indices were used; an overall index; and a resonance-based index. The proposed methodology successfully identified damages as low as 5%. Noise-contaminated FRFs are used, by incorporating a white Gaussian noise. This is done by introducing a signal-to-noise ratio (SNR) of 25 dB into the FRFS to simulate experimental noise. This 25dB is usually considered the minimally acceptable SNR in FRF measurements. The main findings show that the method is simple to implement, as it only requires FRF measurements, and yields notable accuracy in damage detection and localization, supporting broader application of SEM-based techniques in practical SHM.

KEYWORDS: Structural damage, vibration-based method, spectral element method, wave propagation in structures, hybrid approach.

INTRODUCTION

Frame-type structures are integral components in a diverse array of constructions, with extensive applications in industries such as automotive, aerospace, and bridge development, among others. These structures are often subjected to heavy loads and significant levels of vibration, which can potentially result in structural failure due to cracks. One primary source for cracks is fatigue, resulting from repeated loading and unloading cycles. Cracks can also arise from factors like overloading, corrosion, or manufacturing defects. These damages gradually escalate and eventually lead to structural failures. Vibration-based damage diagnosis methods represent a form of energy transmission within a structure, thus enabling methodologies involving energy estimation to be employed in the assessment of structural damage occurrence.

Many methods are implemented for structural damage detection. Some are based on non-destructive testing (NDT), the so-called local methods, including visual inspection, liquid penetrant, radiography, and leak testing. These methods necessitate access to all parts of the structure for inspection, which is impractical for complex systems. In contrast, vibration-based methods offer a global alternative by comparing current dynamic characteristics, such as natural frequencies, mode shapes, and damping ratios, to a baseline state. Building on the principle that structural vibrations represent the

propagation of energy, another class of techniques analyzes how this energy is transmitted, reflected, and attenuated within the structure. One of these is the methodology employing piezoelectric wafer active sensors (PWAS), which is based on using small surface-mounted piezoelectric (PZT) sensors used for SHM, then tracking the propagation of ultrasonic waves generated by PZT emitters [1].

Vibration-based damage detection methods have evolved significantly, incorporating advanced techniques like deep learning, Bayesian frameworks, and hybrid approaches. The integration of deep learning techniques into SHM has been evolving recently from the work of Won *et al*. [2] who proposed an automated structural damage identification method using a 1-D convolutional neural network, to Teng *et al*. [3] who utilized transfer learning with a convolutional neural network to improve damage detection accuracy by up to 47% in complex scenarios. These innovations have improved the accuracy and efficiency of damage detection, making them invaluable tools in structural health monitoring. Bayesian approaches are employed to enhance detection accuracy while minimizing the number of sensor networks. Huang *et al*. [4] introduced a Bayesian probabilistic method that utilizes dynamic responses at a few vibration nodal points, thus allowing for real-time damage assessment with fewer sensors. This method is particularly advantageous for plate structures.

The application of Frequency Response Functions (FRFs) for SHM has been explored through several innovative methodologies. Sajid *et al*. [5] demonstrated the effectiveness of FRF derived from impulse-response tests to detect faults in concrete plates. Their approach involved constructing a feature space matrix based on FRF measurements at specific points, which, when combined with statistical pattern recognition, provided a robust means for identifying defects in concrete structures. Altammar *et al*. [6] introduced an adaptive probabilistic optimization approach that integrates FRF with probabilistic algorithms to assess damage characteristics. This method evaluates the possibility of damage presence, localize it and estimates its severity. Ahmadi *et al*. [7] proposed a different technique that uses Short Time Fourier Transform (STFT) to analyze structure responses subjected to small impact loads, suggesting a damage index derived from FRF analysis with the use of finite element modeling. Naoum *et al*. [8] suggested a wireless real-time SHM by employing piezoelectric materials in fiber-reinforced concrete to monitor flexural cracks. Their method utilized FRF-based indices to assess damage location and severity.

This paper aims to combine FRF data with potential energy, utilizing closed-form expressions for potential energy calculation. The presented work is adopted specifically for frame-type structures, as these closed-form expressions are available for 3D frames at the time being. These expressions are based on exact solutions for wave propagation equations in frames, which involve axial, flexural in two directions, and torsional waveguides. It is important to mention that the term ‘exact’ means that the solution is only limited by the adopted waveguide theory. The solutions are exact in the context of structural wave propagation phenomenon. These solutions are based on the SEM 3D frame elements, i.e. rod, beam and shaft. The main advantage here is that only the experimental FRFs measured at several points of the structure, before and after damage, are required to identify the occurrence and location of damage. Two types of damage indexes are proposed, one as a global index, and the other is based on the contribution of each resonant frequency of the structure. Noise is introduced into the calculated FRFs to

simulate what usually happens in experimental measurements. This noise is introduced as signal-to-noise ratio (SNR) percentage. According to the findings by Presas *et al*. [9], and as known to experimental dynamics community, it is recommended to use reliable, quality FRF measurements in structural dynamics, ideally within an SNR range of 25 dB to 40 dB. This range ensures that the measured signal is sufficiently above the noise floor to yield reliable dynamic analysis. The novelty and main contribution of this work is the development of a hybrid vibration-based damage identification & localization technique that relies solely on measured FRFs.

THEORETICAL FRAMEWORK

Description of the analyzed model

A linear elastic T-beam structure consisting of three spans is used, modeled using the Spectral Element Method (SEM), where each element's dynamic stiffness properties are known. The structure is assumed to be initially intact, and then damage is introduced in the form of a crack represented by a localized reduction in dynamic stiffness. The parameters that are affected are the geometric and material properties. The SEM is formulated in frequency domain, and it describes wave propagation in structures. The governing equation of motion in terms of the dynamic matrix $D(\omega)$ is:

$$[K - \omega^2 M + i\omega C]\{X(\omega)\} = D(\omega)\{X(\omega)\} = \{F(\omega)\} \quad (1)$$

where ω is the excitation frequency, $X(\omega)$ is the displacement response, K, M and C are respectively the stiffness, mass, and damping matrices, and $\{F(\omega)\}$ is the dynamic applied load. In the SEM, K, M and C are not explicitly defined, but they are joined into the dynamic matrix $D(\omega)$. This dynamic matrix changes with the exciting frequency ω. As the SEM is based on exact solution of the wave propagation equation in structures, defined in the form of trigonometric functions, only one element is needed for each uniform span that has the same material and geometry. But in the current case, where damage could be small in size, the mesh would consist of various elements in order to identify the damage location correctly.

The intact T-beam structure used consists of three spans 1.0m each, with uniform cross-section and homogeneous material properties and fixed at two ends, as shown in Figure (1). The beams have the same rectangular cross-section of width b=0.02m, and height h=0.01m.

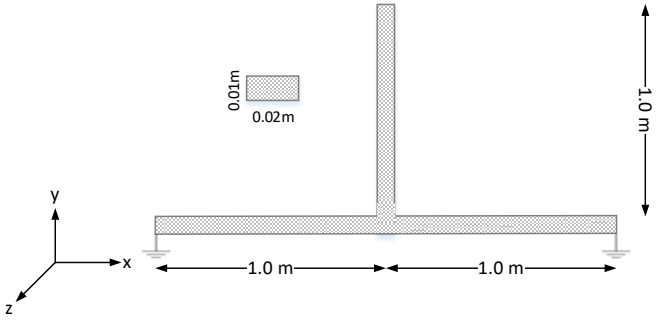

Figure 1: The intact T-beam structure.

Spectral element formulations

The T-beam structure analyzed in this paper could vibrate in all possible directions, i.e., having 3 translations and 3 rotations in the 3D space, as frame structures behave. Thus, it is formulated using elementary rod elements for longitudinal displacement, Bernoulli-Euler beam elements for transverse displacements and rotations in two planes, and shaft elements for in-plane rotation.

Using the SEM, the rod element has the displacements given by Doyle [10]:

$$\hat{u}(x,\omega) = Ae^{-ikx} + Be^{-ik(L-x)} \tag{2}$$

where the symbol ^ denotes a frequency-dependent complex quantity, $\hat{u}(x,\omega)$ is the axial displacement in rod element along any point x along its length, k is the frequency-dependent wave number, L is the element length, and A and B are constants determined by applying the boundary conditions at the 2-noded rod element. The displacement in this form is considered an exact solution to the wave propagation problem in a rod element, limited only by the rod theory used. Applying boundary conditions and using shape functions of a form similar to the finite element method [10], given the nodal displacements $\hat{u}_1$ and $\hat{u}_2$, such that

$$\hat{u}(x) = \hat{g}_1(x)\hat{u}_1 + \hat{g}_2(x)\hat{u}_2 \tag{3}$$

and the shape functions for rod element are given by [10]

$$\begin{aligned} \hat{g}_1(x) &= \left(e^{-ikx} - e^{-ik(2L-x)}\right)/\Delta_1 \\ \hat{g}_2(x) &= -\left(e^{-ik(L+x)} + e^{-ik(L-x)}\right)/\Delta_1 \end{aligned} \tag{4}$$

with $\Delta_1 = 1 - e^{-i2kL}$.

The dynamic stiffness could be related to the nodal forces for a two-node spectral element written in matrix form as:

$$\frac{EA}{L}\frac{ikL}{(1-e^{-i2kL})}\begin{bmatrix} 1+e^{-i2kL} & -2e^{-i2kL} \\ -2e^{-i2kL} & 1+e^{-i2kL} \end{bmatrix}\begin{Bmatrix} \hat{u}_1 \\ \hat{u}_2 \end{Bmatrix} = \begin{Bmatrix} \hat{F}_1 \\ \hat{F}_2 \end{Bmatrix} \tag{5}$$

with E the modulus of elasticity, A the cross-section area, $\hat{u}_1$ and $\hat{u}_2$ are the nodal displacements, and $\hat{F}_1$ and $\hat{\mathrm{F}}_2$ are the nodal applied forces.

Similar symmetric dynamic matrix can be written for shaft element as:

$$\frac{GJ}{L}\frac{ikL}{(1-e^{-i2kL})}\begin{bmatrix} 1+e^{-i2kL} & -2e^{-i2kL} \\ -2e^{-i2kL} & 1+e^{-i2kL} \end{bmatrix}\begin{Bmatrix} \hat{\varphi}_1 \\ \hat{\varphi}_2 \end{Bmatrix} = \begin{Bmatrix} \hat{T}_1 \\ \hat{T}_2 \end{Bmatrix} \tag{6}$$

where G is the torsional modulus of elasticity, J is the polar moment of inertia, $\hat{\varphi}_1$ and $\hat{\varphi}_2$ are the nodal torsional displacements in shaft elements, $\hat{T}_1$ and $\hat{T}_2$ the nodal applied torques in the shaft element.

For Bernoulli-Euler beam element, the dynamic stiffness matrix form is given as:

$$\frac{EI}{L^3}\begin{bmatrix}\hat{k}_{11} & \hat{k}_{12} & \hat{k}_{13} & \hat{k}_{14}\\ \hat{k}_{21} & \hat{k}_{22} & \hat{k}_{23} & \hat{k}_{24}\\ \hat{k}_{31} & \hat{k}_{32} & \hat{k}_{33} & \hat{k}_{34}\\ \hat{k}_{41} & \hat{k}_{42} & \hat{k}_{43} & \hat{k}_{44}\end{bmatrix}\begin{Bmatrix}\hat{v}_1\\ \hat{\phi}_1\\ \hat{v}_2\\ \hat{\phi}_2\end{Bmatrix} = \begin{Bmatrix}\hat{V}_1\\ \hat{M}_1\\ \hat{V}_2\\ \hat{M}_2\end{Bmatrix} \tag{7}$$

where E the Young's modulus, I is the area moment of inertia, $\hat{v}_1$ and $\hat{v}_2$ the flexural displacements, $\hat{\phi}_1$ and $\hat{\phi}_2$ the rotational displacements, $\hat{V}_1$ and $\hat{V}_2$ the nodal applied transverse loads, and $\hat{M}_1$ and $\hat{M}_2$ the nodal applied moments in the beam element. These loads are related to the nodal degrees of freedom (DOF) as: $\hat{V}(x) = EI\frac{\partial^2\hat{\Phi}}{\partial x^2}$ and $\hat{M}(x) = EI\frac{\partial\hat{\Phi}}{\partial x}$, for uniform beams. The individual elements of the Bernoulli-Euler dynamic stiffness matrix are given in the appendix.

Note that all elements of the dynamic stiffness matrices of rod, beam, and shaft elements are complex and functions of excitation frequency. When a frame structure is modeled via SEM, it is divided into a certain number of 2-noded elements. The dynamic stiffness matrices are built in local coordinates for the rod, beam, and shaft elements, and then the global dynamic matrix is assembled. This is done in a fashion similar to finite elements method. Each node will have 6 degrees of freedom. The system is then solved and the displacements are found in global coordinates for all frequency components, and the frequency response is then found for all DOFs.

Modeling frame-type structures using SEM helps predict frequency responses in a reliable manner, especially at high excitation frequencies. The responses are considered *exact* as they depend on *exact* solution of the waveguide governing equation; thus, it is only limited by the adopted waveguide theory. For example, Rayleigh-Love theory for rods gives better solutions compared to the elementary rod theory – as it accounts for the Poisson effect.

Potential energy in frame structures

One of the methodologies frequently used in SHM is the modal strain energy (MSE). It is based on utilizing the MSE coefficient as an indicator for damage occurrence. Nevertheless, the MSE depends mainly on the stiffness matrix and the eigenvectors of the model, which need to be determined a priori. On the other hand, using the current proposed methodology, the calculation of potential energies in each waveguide only depends on having the FRFs at certain DOFs. No stiffness matrices or eigenvectors are needed. When a harmonic excitation is applied, and in the general case of hysteretic damping where the displacements become complex quantities, the potential energy has to be calculated as a time-averaged quantity.

For the rod element, this is done as follows:

$$\langle E_R^P\rangle_t = \frac{1}{2}\int_0^L A\langle Eu'^2\rangle_t dx \tag{8}$$

with $\langle E_R^P\rangle_t$ the time-averaged potential energy and u' is the spatial derivative of the complex displacement along the rod element. Note that the modulus of elasticity becomes a complex quantity in the case of hysteretic damping. This implies that:

$$\langle u'^2\rangle_t = \frac{1}{2}\Re\{\hat{u}'(x)\ \hat{u}'^*(x)\} \tag{9}$$

and thus,

$$\langle E_R^P \rangle_t = \frac{1}{4} A \int_0^L \Re\{E\, \hat{u}'(x)\, \hat{u}'^*(x)\} dx \tag{10}$$

where $\Re$ represents the real part and the * represents the complex conjugate. The rod spectral element shape functions $\hat{g}_i$ and $\hat{g}_j$ are needed to calculate the integrand, as $\hat{u}(x) = \hat{g}_1(x)\hat{u}_1 + \hat{g}_2(x)\hat{u}_2$, and $\hat{u}'(x) = \hat{g}_1'(x)\hat{u}_1 + \hat{g}_2'(x)\hat{u}_2$, given the nodal displacements $\hat{u}_1$ and $\hat{u}_2$. These shape functions for rod element are as follows:

Upon solving the integrands of equation (10), we end up with $\langle E_R^P \rangle_t$ written in a simplified form as:

$$\langle E_R^P \rangle_t = \frac{1}{4} A \Re\{E(E_{dR}^{11}|\hat{u}_1|^2 + E_{dR}^{22}|\hat{u}_2|^2 + E_{dR}^{12}\hat{u}_1\hat{u}_2^* + E_{dR}^{21}\hat{u}_1^*\hat{u}_2)\} \tag{11}$$

where all the terms E_{dR}^{ij} are defined as $E_{dR}^{ij} = \int_0^L \hat{g}'_i \hat{g}'^*_j\, dx$, with i and j =1,2. When hysteretic damping exists, which is the common existing case, Young's modulus becomes complex, written in the form $E \to E(1 + i\eta)$, and the wave number also becomes complex such that $k \to k(\alpha + i\beta)$, with η the loss factor (or hysteretic damping ratio), and α and β are constants. All terms of E_{dR}^{ij} are given in the appendix.

For the shaft element, very similar expressions to the rod element are obtained just be exchanging ρA with ρJ and EA with GJ.

For Bernoulli-Euler beam, similar expressions are obtained for the potential energy, which becomes a bit more complex, by using the same procedure done above for rod and shaft spectral elements. We start by calculating the potential energy as:

$$\langle E_{BB}^P \rangle_t = \frac{1}{2} I \int_0^L \langle E(v'')^2 \rangle_t dx \tag{12}$$

with $\langle E_{BB}^P \rangle_t$ the time-averaged potential energy in the Bernoulli-Euler spectral beam element, and v'' is the 2nd spatial derivative of the transverse displacement. The shape functions in Bernoulli-Euler beam are used for obtaining the derivatives and integrals, where the displacement at an arbitrary point along the beam, and its spatial derivative, can be found as follows, respectively:

$$\hat{v}(x) = \hat{g}_1(x)\hat{v}_1 + \hat{g}_2(x)\hat{\Phi}_1 + \hat{g}_3(x)\hat{v}_2 + \hat{g}_4(x)\hat{\Phi}_2 \tag{13}$$

$$\hat{v}''(x) = \hat{g}_1''(x)\hat{v}_1 + \hat{g}_2''(x)\hat{\Phi}_1 + \hat{g}_3''(x)\hat{v}_2 + \hat{g}_4''(x)\hat{\Phi}_2 \tag{14}$$

The shape functions for Bernoulli-Euler beam are defined as:

$$\begin{Bmatrix} \hat{g}_1(x) \\ \hat{g}_2(x) \\ \hat{g}_3(x) \\ \hat{g}_4(x) \end{Bmatrix} = \frac{1}{\Delta_3} \begin{bmatrix} r_1 & r_2 & 0 & 0 \\ 0 & 0 & r_1 & r_2 \\ r_2 & r_1 & 0 & 0 \\ 0 & 0 & -r_2 & -r_1 \end{bmatrix} \begin{Bmatrix} \hat{h}_1(x) \\ \hat{h}_2(x) \\ \hat{h}_3(x) \\ \hat{h}_4(x) \end{Bmatrix} = \frac{1}{\Delta_3} [r]\{\hat{h}(x)\} \tag{15}$$

with $\Delta_3 = -r_1^2 + r_2^2$, $r_1 = i(k_1 - k_2)\left(1 - e^{-ik_1L}e^{-ik_2L}\right)$, $r_2 = i(k_1 + k_2)(e^{-ik_1L} - e^{-ik_2L})$, $k_1 = k$, $k_2 = -ik$, and

$$\hat{h}_1(x) = ik_2\left(e^{-ik_1x} - e^{-ik_2L}e^{-ik_1(L-x)}\right) - ik_1\left(e^{-ik_2x} - e^{-ik_1L}e^{-ik_2(L-x)}\right)$$
$$\hat{h}_2(x) = -ik_2\left(e^{-ik_2L}e^{-ik_1x} - e^{-ik_1(L-x)}\right) + ik_1\left(e^{-ik_1L}e^{-ik_2x} - e^{-ik_2(L-x)}\right)$$
$$\hat{h}_3(x) = \left(e^{-ik_1x} + e^{-ik_2L}e^{-ik_1(L-x)}\right) - \left(e^{-ik_2x} + e^{-ik_1L}e^{-ik_2(L-x)}\right)$$
$$\hat{h}_4(x) = \left(e^{-ik_2L}e^{-ik_1x} + e^{-ik_1(L-x)}\right) - \left(e^{-ik_1L}e^{-ik_2x} + e^{-ik_2(L-x)}\right).$$

Plugging these shape functions into equation (12) and solving the integrations, we end up with the equation for time-averaged potential energy $\langle E_{BB}^P \rangle_t$ as:

$$\begin{aligned}\langle E_{BB}^P \rangle_t = \frac{1}{4}\omega^2 I\Re\{E(&E_{dB}^{11}|\hat{v}_1|^2 + E_{dB}^{12}\hat{v}_1\hat{\varphi}_1^* + E_{dB}^{13}\hat{v}_1\hat{v}_2^* + E_{dB}^{14}\hat{v}_1\hat{\varphi}_2^* + \\ &E_{dB}^{21}\hat{\varphi}_1\hat{v}_1 + E_{dB}^{22}|\hat{\varphi}_1|^2 + E_{dB}^{23}\hat{\varphi}_1\hat{v}_2 + E_{dB}^{24}\hat{\varphi}_1\hat{\varphi}_2 + \\ &E_{dB}^{31}\hat{v}_2\hat{v}_1 + E_{dB}^{32}\hat{v}_2\hat{\varphi}_1 + E_{dB}^{33}|\hat{v}_2|^2 + E_{dB}^{34}\hat{v}_2\hat{\varphi}_2 + \\ &E_{dB}^{41}\hat{\varphi}_2\hat{v}_1 + E_{dB}^{42}\hat{\varphi}_2\hat{\varphi}_1 + E_{dB}^{43}\hat{\varphi}_2\hat{v}_2 + E_{dB}^{44}|\hat{\varphi}_2|^2)\}\end{aligned} \tag{16}$$

where every term is defined by, with H denoting Hermitian matrix:

$$\begin{bmatrix} E_{dB}^{11} & E_{dB}^{12} & E_{dB}^{13} & E_{dB}^{14} \\ E_{dB}^{21} & E_{dB}^{22} & E_{dB}^{23} & E_{dB}^{24} \\ E_{dB}^{31} & E_{dB}^{32} & E_{dB}^{33} & E_{dB}^{34} \\ E_{dB}^{41} & E_{dB}^{42} & E_{dB}^{43} & E_{dB}^{44} \end{bmatrix} = \frac{1}{|\Delta|^2}[r]\left[\int_0^L \{h''\}\{h''\}^H dx\right][r]^H = \frac{1}{|\Delta|^2}[r]\,[N1]\,[r]^H \tag{17}$$

and all the involved and resulting terms are defined in the appendix. Note that the matrix E_{dB}^{ij} is symmetric, which facilitates its computation using specialized algorithms, if desired.

METHODOLOGY TO IDENTIFY STRUCTURAL DAMAGE

The framework used for identifying the occurrence and localization of damage is based on calculating the time-averaged change in potential energies in all members of the structure. All these energy expressions given above need frequency responses calculated at all selected DOFs. The algorithm is defined as follows:

- Build a model that represents the intact structure using the SEM, using a sufficient number of elements. The number of elements depends on how accurately the damage location is to be identified.
  - Calculate the frequency responses at all DOFs. ***In a real case scenario, these are the experimentally measured frequency responses of the intact structure***. But as this paper deals with numerical experiment, the numerical FRFs are used instead.
  - Calculate the potential energies in all elements using the frequency responses and the aforementioned expressions, i.e., rod, beam in two planes, and shaft waveguides.
  - For the sake of simulation, damage is introduced in selected elements by changing their material and geometric parameters by a certain percentage.
  - Calculate the frequency responses again at all DOFs. In a real case scenario, these are measurements taken to verify the occurrence of structural faults.
  - Calculate the potential energies again in all elements.
  - Identify the damage location using the damage localization index, described below.

Damage localization algorithm

Overall damage localization index (DLI_e):

For a given frequency range containing some resonances, the average potential energy $\overline{U}_e$ is calculated for each element, using equation (18). This is to find which elements are storing the most energy over the defined frequency range.

$$\overline{U}_e = \frac{1}{N}\sum_{i=1}^{N} U_e(\omega_i) \tag{18}$$

where $\overline{U}_e$ is the element potential energy averaged over a given frequency range of N points, and U_e is the element potential energy at ω_i. The difference between the magnitudes of energies of the intact and damaged models, for each element, is used as a damage localization index (DLI_e). This index is calculated then normalized by the maximum of the intact energy value, as:

$$DLI_e = \left|\frac{\overline{U}_e^i - \overline{U}_e^d}{\overline{U}_e^i}\right| \tag{19}$$

where $\overline{U}_e^i$ is the average potential energy of element e of the intact structure, and $\overline{U}_e^d$ is the average potential energy for the damaged element. Higher DLI_e tells which elements, on average, have (are storing) the most potential energy, thus are most likely suffer from damages. It is important to mention that adjacent elements could also have high DLI_e.

Resonance-based damage localization index ($DLIr_e$):

This is also based on comparing energies before and after damage, but mainly focuses on the changes at or near the resonant frequency, where potential energy change is most pronounced. The procedure is as follows:

- Calculate the energy change for each element e and at each frequency ω_i, and normalize it by the energy of the intact structure
$$\Delta U_e(\omega_i) = \left|U_e^i(\omega_i) - U_e^d(\omega_i)/U_e^i(\omega_i)\right|$$
- Identify the resonances of the intact structure ω_r. In this paper, no more than the first 10 resonances are utilized.
- For each ω_r calculate $DLIr_e$, which is a DLI mapping at each resonant frequency for each element e.
- Create a 3D bar plot of $DLIr_e$ to show the *"hotspots"*, where the energy change is shown at different elements, at certain resonances. This makes it possible to see the contribution of every element at each resonance.

NUMERICAL SIMULATIONS

For these simulations, a code was written in MATLAB® environment. The T-beam structure of Figure (1) is modeled via SEM. It is made of stainless-steel members with the following properties: A=0.02×0.01m^2, ρ=7800 kg/m^3, E=210GPa, η=0.03, and ν=0.3. A total of 40 elements are used, resulting in 41 nodes, each node with 6 DOFs. Loads are applied at the tip of the vertical member, where all possible loads are used. These loads are impulse-type loads in time that excite all resonances in the analyzed frequency range. These are represented by a spectrum of a unitary constant value in the frequency domain, across all frequencies. The two ends of the horizontal members are clamped to the ground, as shown in Figure (2).

To investigate a structural damage case, non-propagating cracks are considered. This is done by introducing changes in geometric and material properties in few elements, with different damage percentages. Elements 6 & 30 suffer from 10% change in its parameters, and element 38 from 5% change. The elements indices and severity of damages are as indicated in Table (1) and Figure (2). The other parameters are: polar moment of inertia (Jp), moment of inertia about the y-axis (Iy), and moment of inertia about the z-axis (Iz).

Table 1: Indices of damaged elements with their corresponding parameters values.

Element No.	Geometric parameters		Material parameters		Change
	Intact	damaged	Intact	Damaged	
6 & 30	A=2.0e-4 m^2 Jp=4.576e-9 m^4 Iy=6.666e-9 m^4 Iz=1.666e-9 m^4	A=1.80e-4 m^2 Jp=4.1184e-9 m^4 Iy=6.000e-9 m^4 Iz=1.500e-9 m^4	E=2.1e11 Pa	E=189.0e9 Pa	10%
38		A=1.90e-4 m^2 Jp=4.3472e-9 m^4 6.33334e-9 m^4 1.58334e-9 m^4		E=199.5e9 Pa	5%

Structural damage could affect structures in many ways, from local tiny cracks to causing a geometrical discontinuity. In the current case, we are dealing with smaller damages in frame structures. The direct effect of small damage is the reduction in cross-sectional area, and hence the reduction of elastic moduli of elasticity and moments of inertia [12,13]. Note that the mass density is kept unchanged as the material is the same with or without damage.

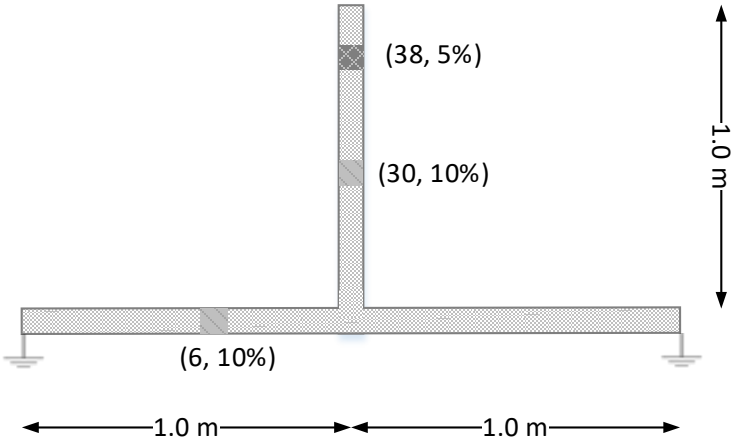

Figure 2: The T-beam structure with damaged elements (element No., damage %).

Results and discussion

The intact model of Figure (1) is run, and the potential energies in all elements and the resonances are all recorded. Then the model with damages, Figure (2), is run, and the energies data are recorded. A frequency range of 0-2000Hz with a 0.5Hz step is utilized. This range encompasses about 13 resonances. As a result of the built algorithms, the FRF is calculated at all existing DOFs in the model (246 DOFs). The averaging of all FRFs is done by superposing responses calculated as RMS over all DOFs N, using equation (20), and is shown in Figure (3). Note that f is the frequency in Hz, N is the number of frequency steps, and H is the frequency response function.

$$H_{rms}(f) = \sqrt{\frac{1}{N}\sum_{i=1}^{N}|H_i(f)|^2} \tag{20}$$

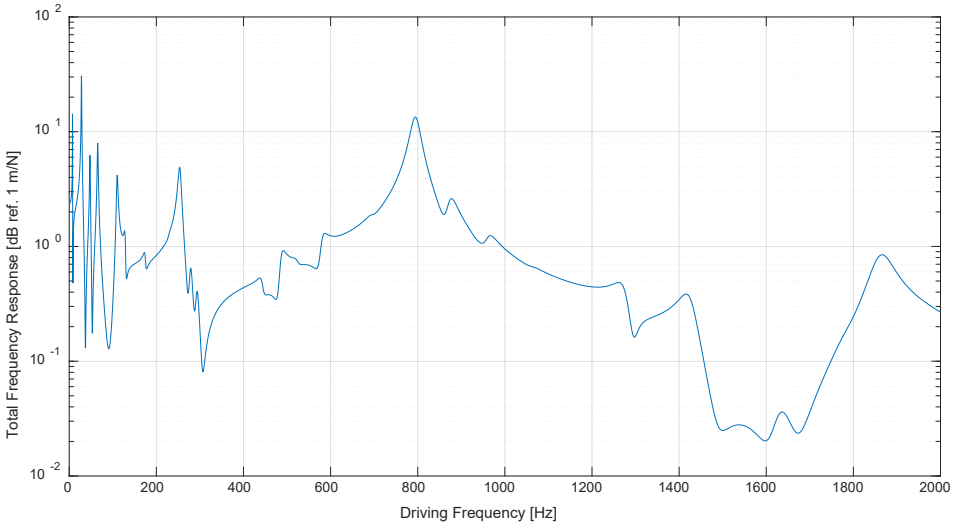

Figure 3: The total frequency response of the intact structure.

As expected, the natural frequencies of the structure have changed (decreased) due to damage, as in Table (2). Although this indicates a change in structural integrity, it alone may not be sufficient to pinpoint the location of the damage.

Table 2: Natural frequencies (Hz) of the structure: intact and damaged.

Nat. Freq. No.	1	2	3	4	5	6	7	8	9	10
Intact model	7.48	28.15	47.55	65.39	110.20	126.87	171.56	253.49	277.86	293.04
Damaged model	7.48	28.24	47.29	65.18	109.80	126.34	170.03	253.21	275.54	292.08

Using these FRFs, the aforementioned overall damage localization index (DLI_e) is calculated and shown for all elements, as demonstrated in Figure (4). It is clearly observed how the proposed methodology detects the damaged elements, even elements with only 5% damage severity. The neighboring elements, say neighbors of element 6, also show a

little high DLI_e. This is a consequence of how localized cracks affect the overall stiffness and strain distribution of the structure. Refining the SEM mesh, especially around suspected regions, could help the localization of damage more precisely.

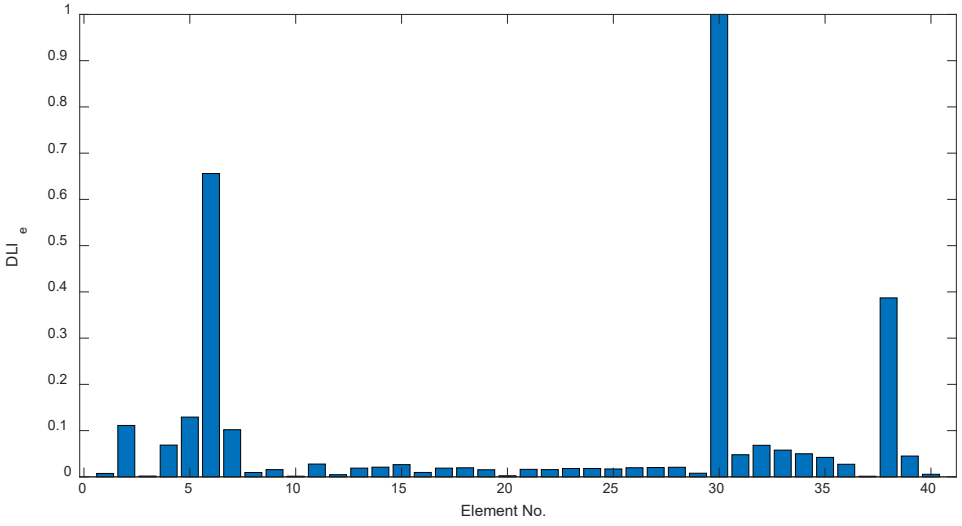

Figure 4: Overall damage localization index DLI_e in the T-Beam structure.

Besides that, the resonance-based damage localization index $DLIr_e$ is 3D-plotted to show the hotspots where variation of potential energy is shown at the first 10 resonances. This is a demonstration of the sensitivity of $DLIr_e$ to resonant frequency, and of the contribution of each resonance (mode shape) in the DLI index, as in Figure (5).

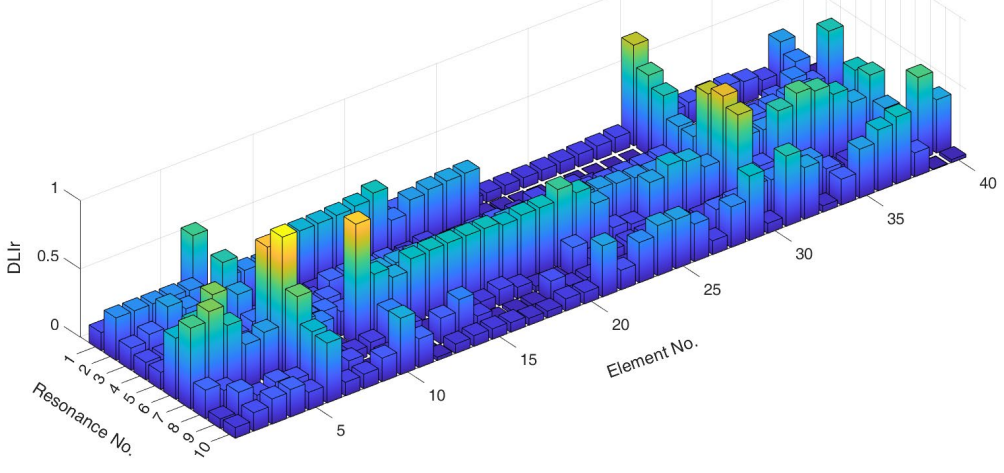

Figure 5: Resonance-based damage localization index $DLIr_e$.

REMARKS ON THE PROPOSED METHODOLOGY

- To calculate the overall damage localization index DLI_e, only the FRFs measured at some points on the analyzed structure are needed.
- If the index $DLIr_e$ is required for detailed analysis, then the FRFs and resonances are needed.

- Real experimentally-measured FRFs can be used by plugging the measured displacements and rotations into the closed-form expressions of the potential energy, then applying the algorithms for $\mathrm{DLI_e}$ (and $\mathrm{DLIr_e}$ $if\ needed$), and identifying damages, if any.
- When experimental data is used, each span between two measurement points is called "element" with a certain length L, in analogy to the SEM mesh and elements.
- Solely translational DOFs can be used in the analysis when the rotational DOFs are hard to measure.
- If it becomes necessary to include rotational DOFs, due to the structure's type or type of applied loads, then a methodology already exists for obtaining these rotational DOFs out of the translational displacements, as explained by Ahmida and Arruda [14].
- For better localization of damages, a finer mesh is always appreciated.
- Analyzing the contribution of every resonance could become necessary for the damage identification process, or for deeper understanding of resonances contributions.
- The used number of resonances might, in general, influence the effectiveness of damage detection algorithm. A key parameter could be the use of many resonances in the analysis, thus providing a richer feature set for damage identification [5,15,16].

ANALYSIS WITH NOISE-CONTAMINATED FRF

In general, vibration-based damage detection methods are susceptible to noise contamination. The proposed methodology presented in this paper is not an exception, as observed from what follows. Other methods, for instance, the MSE method that depends on mode shapes, are perturbed by noise contained in measurements, leading to crests when calculating modal curvature [12]. The limitation of mode-shape-based methods is observed when higher mode shapes are extracted from noisy measurements, and these methods could then become impractical. Generally, the effect of noise contamination can be decreased by increasing the FRF sampling points and employing a suitable frequency increment. The effect of noise can also be alleviated by using noise reduction techniques, as explained by Cao *et al*. [17].

In the current proposed methodology, using $\mathrm{DLI_e}$ and $\mathrm{DLIr_e}$ indices, numerical experiments were conducted to mimic noise-polluted FRFs. Noise is incorporated into the obtained FRFs of both intact and damaged structures by using a signal-to-noise ratio (SNR) that accounts for noise contamination. A white Gaussian noise is added to the numerically obtained FRFs. This white Gaussian noise has a flat power spectral density across the entire frequency spectrum.

A simple cantilever beam is used as a case study. The beam has a length L=1.0m, and the same geometry and material properties as for the T-beam analyzed above. The cantilever beam is modeled with 10 SEM elements, with unitary flat spectrum force and moment applied at its free end, see Figure (6). The FRF is calculated at all the DOFs in its healthy and damaged cases. Then an SNR of 25 dB is introduced into the FRFs to simulate experimental noise. A good range of noise for reliable performance often recommended is 25 dB to 40 dB. The 25 dB is usually considered the minimally acceptable ratio in FRF measurements [18,19]. The superposed response calculated as RMS over all N DOFs for 1-400 Hz is shown in Figure (7).

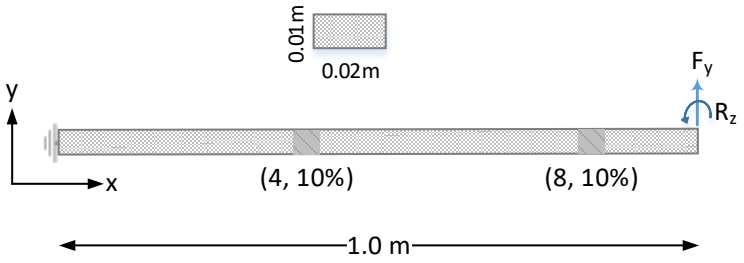

Figure 6: The cantilever beam with two damaged elements (element No., damage %).

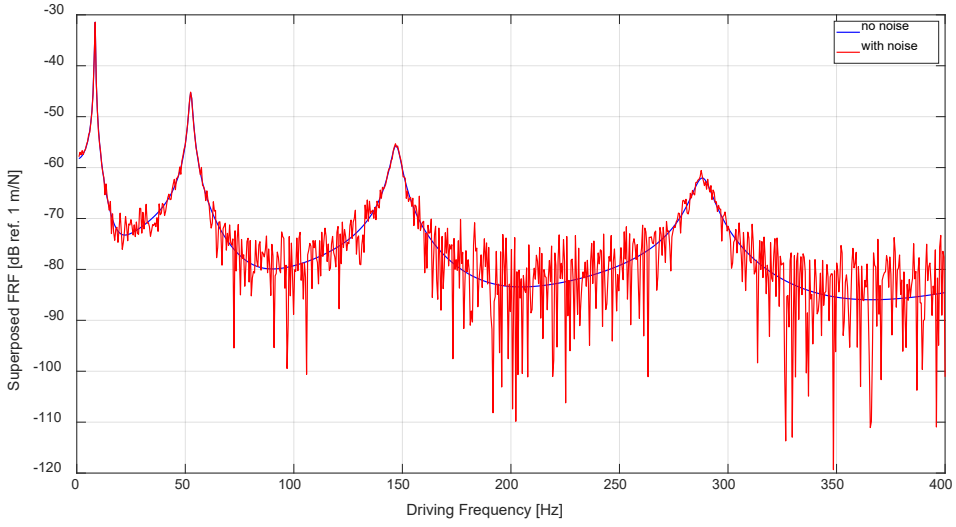

Figure 7: The FRF of the intact cantilever beam, without noise and with an SNR of 25 dB.

Different frequency ranges and frequency step sizes are analyzed. The DLI_e index is calculated and compared for each case, as demonstrated in Figs. 8,9, and 10.

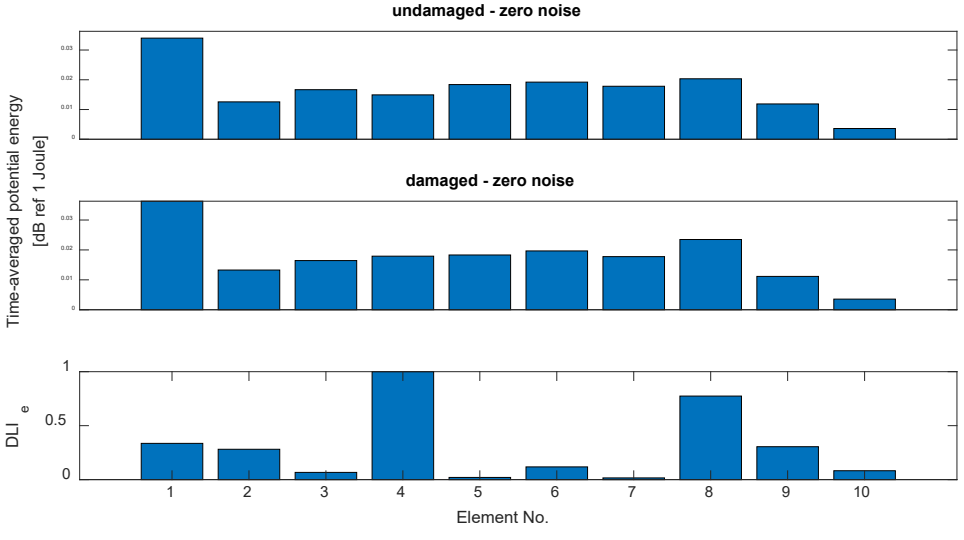

Figure 8: The DLI_e for the cantilever beam: with zero noise.

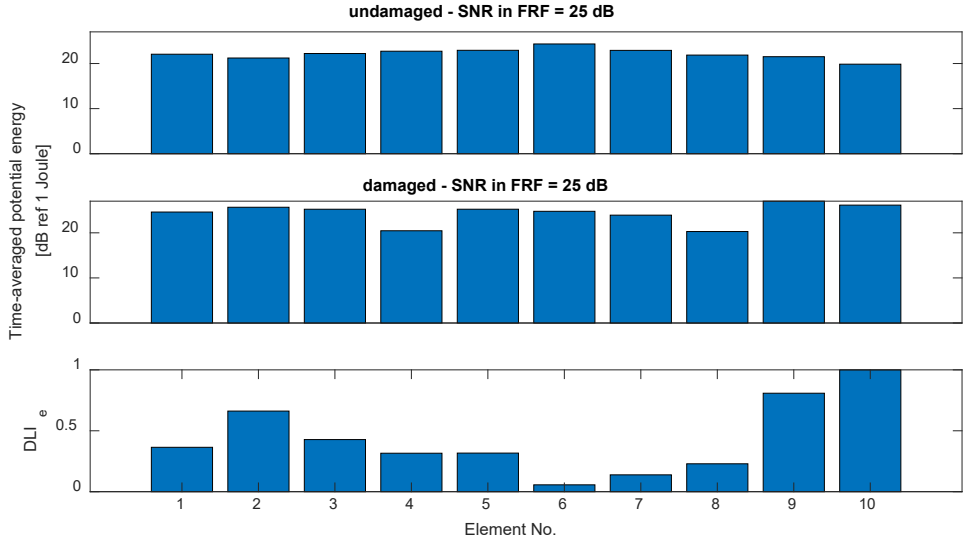

Figure 9: The DLI_e for the cantilever beam: with SNR of 25dB and

1 to 400 Hz (400 points).

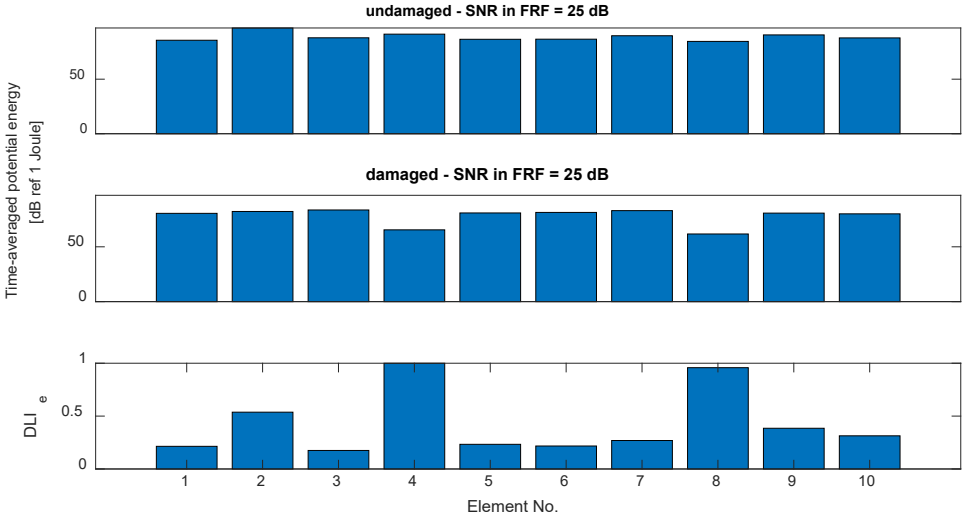

Figure 10: The DLI_e for the cantilever beam: with SNR of 25dB and 1 to 200 Hz (400 points).

The effect of noise in FRFs on the estimation of the index DLI_e is as depicted in Figure (8). For noise-clean FRF, the estimation of DLI_e is notably good (Figure 8). The SNR of 25 dB clearly affected the identification of damages (Figure 9). Nevertheless, using only the first three resonances with a sufficient frequency step-size enabled the identification of damages in elements 4 & 8 (Figure 10). These findings could be affected by the type of structure in question, and require deeper investigation supported by real experimental measurements.

CONCLUSIONS

This study provides a different approach to using FRF for damage detection. It does not depend on analyzing resonances and mode shapes, as many approaches do, nor it depend on stiffness matrix and mode shapes as in modal strain energy (MSE) methods that require a priori the identification of mode shapes. It as well does not use advanced approaches like deep learning or Bayesian frameworks. The proposed method simply relies on closed-form expressions for the calculation of potential energies in 3D frame structures. These expressions are obtained by using the Spectral Element Method (SEM) formulations considering all waveguide types, i.e. axial, transversal, and rotational. On the basis of these, the indices for damage localization are found. This method only requires the frequency response functions (FRFs) measured at several points across the structure. Then, these FRFs are plugged into the potential energy expressions, and the change in energies is used via the proposed damage localization indexes. The main advantage of this methodology is the possibility of directly using experimentally measured FRFs. No identification of resonances is necessary, unless the contribution of these resonances in calculating the damage localization index is required. The overall damage localization index (DLI_e) has shown success in identifying and localizing damages, even in the presence of a relatively acceptable signal-to-noise ratio. These results are due to the *exact* nature of the SEM solutions, which are based on wave propagation in structures. If the FRF is noise-contaminated, then employing responses that include only the first few resonances seems to overcome the noise issues to a certain degree. However, high SNR FRFs of 40 dB or more are always recommended. The obtained results contribute towards best practices for enhancing the use of SEM in SHM. This work contributes in introducing novel FRF-driven expressions for damage identification & localization in 3D frame structures. Future work is recommended to include plate/shell-type structures.

ABBREVIATIONS

DLI	Damage Localization Index
DLIe	Overall Damage Localization Index
DLIre	Resonance-based Damage Localization Index
DOF	Degree of Freedom
FRF	Frequency Response Function
MSE	Modal Strain Energy
NDT	Non-Destructive Testing
PWAS	Piezoelectric Wafer Active Sensors
PZT	Piezo-electric Transducer
RMS	Root Mean Square
STFT	Short Time Fourier Transform
SNR	Signal-to-Noise Ratio
Ue	Potential energy per element

DECLARATION OF CONFLICTING INTERESTS

The author declares no potential conflicts of interest with respect to the research, authorship, and/or publication of this article.

FUNDING

The author received no financial support for the research, authorship, and/or publication of this article.

DECLARATION OF GENERATIVE AI AND AI-ASSISTED TECHNOLOGIES IN THE WRITING PROCESS

During the preparation of this work, the author did not use any generative AI or AI-assisted technologies in the writing process.

REFERENCES

[1] Giurgiutiu V (2008) Piezoelectric wafer active sensors. *In: Structural health monitoring with piezoelectric wafer active sensors*, 239-247, Columbia, SC, USA.

[2] Won J, Park J W, Jang S, Jin K and Kim Y (2021) Automated structural damage identification using data normalization and 1-dimensional convolutional neural network. *Applied Sciences* 11(6): 2610.

[3] Teng S, Chen G, Yan Z, Cheng L and Bassir D (2022) Vibration-based structural damage detection using 1-D convolutional neural network and transfer learning. *Structural Health Monitoring* 22(4): 2888-2909. https://doi.org/10.1177/14759217221137931

[4] Huang T and Schröder K (2021) A Bayesian probabilistic approach for damage identification in plate structures using responses at vibration nodes. *Mechanical systems and Signal Processing* 146. https://doi.org/10.1016/j.ymssp.2020.106998

[5] Sajid S, Taras A and Chouinard L (2021) Defect detection in concrete plates with impulse-response test and statistical pattern recognition. *Mechanical Systems and Signal Processing* 161. doi.org/10.1016/j.ymssp.2021.107948.

[6] Altammar H and Kaul S (2021) Adaptive probabilistic optimization approach for vibration-based structural health monitoring. *Signals* 2(3): 475-489.

[7] Ahmadi H R, Mahdavi N and Bayat M (2021) A novel damage identification method based on short time Fourier transform and a new efficient index. *Structures* 33(4): 3605-3614.

[8] Naoum M C, Papadopoulos N A, Voutetaki M E and Chalioris C (2023) Structural health monitoring of fiber-reinforced concrete prisms with polyolefin macro-fibers using a piezoelectric materials network under various load-induced stress. *Buildings* 13(10): 2465. https://doi.org/10.3390/buildings13102465

[9] Presas A, Valentin D, Egusquiza E, Valero C, Egusquiza M and Bossio M (2017) Accurate determination of the frequency response function of submerged and confined structures by using PZT-patches. *Sensors* 17(3): 660. doi.org/10.3390/s17030660

[10] Doyle J F (1997) Wave propagation in structures: a spectral analysis approach. 2nd Ed., Cambridge University Press.

[11] Ahmida K M (2023) Novel closed-form expressions for potential energy estimation in 3D, Springer Nature. *Journal of the Brazilian Society of Mechanical Sciences and Engineering* 45: 529. doi.org/10.1007/s40430-023-04446-w

[12] Sun X, Ilanko S, Mochida Y and Tighe, R C (2023) A review on vibration-based damage detection methods for civil structures. *Vibration* 6: 843-875.
[13] Ghazi R M and Buyukozturk O (2014) Assessment and localization of active discontinuities using energy distribution between intrinsic modes. *In: Structural Health Monitoring*, v5, the 32nd IMAC, Conference proceedings of the Society for Experimental Mechanics Series.
[14] Ahmida K M and Arruda J R F (2003) Exact modelling of kinetic energy in truss-type members. *Journal of Sound and Vibration* 267(1): 167-177. doi.org/10.1016/S0022-460X(03)00153-6
[15] Tavares A, Peeters B, Coppotelli G and Silvestre N (2021) Damage detection in lightweight structures using artificial intelligence techniques. *Experimental Techniques* 45:1-22. doi.org/10.1007/s40799-020-00421-5
[16] Das S and Roy K (2021) A State-of-the-Art Review on FRF-based structural damage detection: development in last two decades and way forward. *International Journal of Structural Stability and Dynamics* 22. doi.org/10.1142/S0219455422300014.
[17] Cao M, Xu W, Ren W, Ostachowicz W, Sha G and Pan L A (2016) Concept of complex-wavelet modal curvature for detecting multiple cracks in beams under noisy conditions. *Mechanical Systems and Signal Processing* 76: 555-575.
[18] Avitabile P (2001) Experimental modal analysis: A simple non-mathematical presentation. *Sound and Vibration* 35: 20-31.
[19] Zar A, Hussain Z, Akbar M, Rabczuk T, Lin Z, Li S and Ahmed B (2024) Towards vibration-based damage detection of civil engineering structures: overview, challenges, and future prospects. *International Journal of Mechanics and Materials in Design* 20:591-662. doi.org/10.1007/s10999-023-09692-3.

APPENDIX

Elements of Bernoulli-Euler beam dynamic stiffness matrix:

$\hat{k}_{11} = (z_{11}z_{22} - iz_{12}z_{21})\xi^3/\Delta$, $\hat{k}_{12} = 0.5(i+1)(z_{12}^2 - z_{11}^2)\xi^2 L/\Delta$, $\hat{k}_{13} = (iz_{12}z_{22} - z_{11}z_{21})\xi^3/\Delta$, $\hat{k}_{14} = -(1-i)z_{11}z_{12}\xi^2 L/\Delta$, $\hat{k}_{22} = (iz_{11}z_{22} - z_{12}z_{21})\xi L^2/\Delta$, $\hat{k}_{23} = -\hat{k}_{14}$,

$\hat{k}_{24} = (z_{12}z_{22} - iz_{11}z_{21})\xi L^2/\Delta$, $\hat{k}_{33} = \hat{k}_{11}$, $\hat{k}_{34} = -\hat{k}_{12}$, $\hat{k}_{44} = \hat{k}_{22}$, $\xi = kL$

$z_{11} = \left(1 - e^{-i\xi}e^{\xi}\right)$, $z_{12} = (e^{-i\xi} - e^{\xi})$, $z_{21} = (e^{-i\xi} + e^{\xi})$, $z_{22} = \left(1 + e^{-i\xi}e^{\xi}\right)$

$\Delta = \frac{(z_{11}^2 + z_{12}^2)}{(1+i)}$.

Potential energy terms E_{dR}^{ij} for rod element with hysteretic damping:

$$E_{dR}^{11} = -\frac{\left(i\beta e^{2\beta L} - i\beta e^{2L(2i\alpha+\beta)} - e^{2i\alpha L}\alpha + \alpha e^{2L(i\alpha+2\beta)}\right)\left(\alpha^2+\beta^2\right)}{2\alpha\beta\left(e^{2L(2i\alpha+\beta)} - e^{2L(i\alpha+2\beta)} - e^{2i\alpha L} + e^{2\beta L}\right)}$$

$$E_{dR}^{12} = \frac{\left(\alpha^2+\beta^2\right)\left((-i\beta-\alpha)e^{L(i\alpha+3\beta)} + (i\beta+\alpha)e^{L(3i\alpha+\beta)} + (i\beta-\alpha)\left(e^{3L(i\alpha+\beta)} - e^{L(i\alpha+\beta)}\right)\right)}{2(-e^{2i\alpha L} + e^{2\beta L})(-1 + e^{2L(i\alpha+\beta)})\alpha\beta}$$

$E_{dR}^{21} = E_{dR}^{12}$ and $E_{dR}^{22} = E_{dR}^{11}$.

Potential energy terms E_{dB}^{ij} for beam element, and involved terms:

$\Delta = -r_1^2 + r_2^2,\ k_1 = k,\quad k_2 = -ik,\ r_1 = i(k_1 - k_2)(1 - e^{-ik_1 L}e^{-ik_2 L}),\ r_2 = i(k_1 + k_2)(e^{-ik_1 L} - e^{-ik_2 L})$

$\hat{h}_1(x) = ik_2\left(e^{-ik_1 x} - e^{-ik_2 L}e^{-ik_1(L-x)}\right) - ik_1\left(e^{-ik_2 x} - e^{-ik_1 L}e^{-ik_2(L-x)}\right)$

$\hat{h}_2(x) = -ik_2\left(e^{-ik_2 L}e^{-ik_1 x} - e^{-ik_1(L-x)}\right) + ik_1\left(e^{-ik_1 L}e^{-ik_2 x} - e^{-ik_2(L-x)}\right)$

$\hat{h}_3(x) = \left(e^{-ik_1 x} + e^{-ik_2 L}e^{-ik_1(L-x)}\right) - \left(e^{-ik_2 x} + e^{-ik_1 L}e^{-ik_2(L-x)}\right)$

$\hat{h}_4(x) = \left(e^{-ik_2 L}e^{-ik_1 x} + e^{-ik_1(L-x)}\right) - \left(e^{-ik_1 L}e^{-ik_2 x} + e^{-ik_2(L-x)}\right)$

Elements of matrix the symmetric N1:

$$N1(1,1) = -\frac{\left((I\beta - I\alpha)e^{-L((1+I)\alpha+(-1+I)\beta)} + (-I\beta + I\alpha)e^{((-1+I)\alpha+(1+I)\beta)L} + (I\beta + I\alpha)e^{(1+I)L(-\alpha+\beta)} + (-I\beta - I\alpha)e^{(-1+I)L(\alpha-\beta)}\right)\left(\alpha^2+\beta^2\right)^4}{-2\alpha^3\beta + 2\alpha\beta^3} + \frac{((\alpha+\beta)e^{-2L(\alpha-\beta)} + (-\alpha+\beta)e^{-2\alpha L} + (\alpha-\beta)e^{2\beta L} - \beta - \alpha)\left(\alpha^2+\beta^2\right)^4}{-2\alpha^3\beta + 2\alpha\beta^3}$$

$$N1(1,2) = -\frac{(\alpha^2+\beta^2)^4\left(-(1+I)\beta e^{-((2+I)\alpha-\beta)L} - (1+I)\alpha e^{((2+I)\beta-\alpha)L} + (1-I)\beta e^{-L(I\alpha-\beta)} + (-1+I)\alpha e^{-L((-2+I)\beta+\alpha)}\right)}{-2\alpha^3\beta + 2\alpha\beta^3} + \frac{(\alpha^2+\beta^2)^4((1-I)\alpha e^{L(I\beta-\alpha)} + (-1+I)\beta e^{L((-2+I)\alpha+\beta)} + (1+I)\alpha e^{-L(I\beta+\alpha)} + (1+I)e^{L(I\alpha+\beta)}\beta)}{-2\alpha^3\beta + 2\alpha\beta^3}$$

$$N1(1,3) = \frac{\left(\alpha^2+\beta^2\right)^3\left(e^{-((1+I)\alpha+(-1+I)\beta)L} + e^{2\beta L} + e^{-2\alpha L} - e^{-2L(\alpha-\beta)} - e^{(1+I)L(-\alpha+\beta)} - e^{(-1+I)L(\alpha-\beta)} + e^{L((-1+I)\alpha+(1+I)\beta)} - 1\right)}{2\beta\alpha}$$

$$N1(1,4) = \frac{\left(\alpha^2+\beta^2\right)^3\left(e^{-L((-2+I)\beta+\alpha)} - e^{-((2+I)\alpha-\beta)L} - e^{L(I\alpha+\beta)} + e^{L(I\beta-\alpha)} - e^{-L(I\alpha-\beta)} + e^{-L(I\beta+\alpha)} + e^{((2+I)\beta-\alpha)L} - e^{L((-2+I)\alpha+\beta)}\right)}{-\alpha^2+\beta^2}$$

$N1(2,2) = N1(1,1)$

$N1(2,3) = N1(1,4)$

$N1(2,4) = N1(1,3)$

$$N1(3,3) = \frac{\left(\alpha^2+\beta^2\right)^2\left(I(-\alpha+\beta)(\alpha^2+4\beta\alpha+\beta^2)e^{-L((1+I)\alpha+(-1+I)\beta)} - I(-\alpha+\beta)(\alpha^2+4\beta\alpha+\beta^2)e^{L((-1+I)\alpha+(1+I)\beta)}\right)}{-2\alpha^3\beta + 2\alpha\beta^3} \ldots$$

$$+\frac{\left(\alpha^2+\beta^2\right)^2\left(I(\alpha+\beta)(\alpha^2-4\beta\alpha+\beta^2)e^{(1+I)L(-\alpha+\beta))} - I(\alpha+\beta)e^{(-1+I)L(\alpha-\beta)}\right)}{-2\alpha^3\beta + 2\alpha\beta^3} \ldots$$

$$+\frac{\left(\alpha^2+\beta^2\right)^2\left((-\alpha^3+3\alpha^2\beta+3\alpha\beta^2-\beta^3)e^{-2L(\alpha-\beta)} + (\alpha^3+3\alpha^2\beta-3\alpha\beta^2-\beta^3)e^{-2\alpha L} + (-\alpha+\beta)(\alpha^2+4\beta\alpha+\beta^2)e^{2\beta L} + (\alpha+\beta)(\alpha^2-4\beta\alpha+\beta^2)\right)}{-2\alpha^3\beta + 2\alpha\beta^3}$$

$N1(3,4)$

$$= \frac{3\left(\alpha^2+\beta^2\right)^2\left(\left(-\frac{1}{3}+\frac{I}{3}\right)\beta(-3\alpha^2+\beta^2)e^{-((2+I)\alpha-\beta)L}+(1-I)\left(\beta^2-\frac{\alpha^2}{3}\right)\alpha e^{L((2+I)\beta-\alpha)}+\left(\frac{1}{3}+\frac{I}{3}\right)\beta(-3\alpha^2+\beta^2)e^{-L(I\alpha-\beta)}+(1+I)\left(\beta^2-\frac{\alpha^2}{3}\right)\alpha e^{-((-2+I)\beta+\alpha)L}\right)}{-2\alpha^3\beta+2\alpha\beta^3}\ldots$$

$$-\frac{3\left(\alpha^2+\beta^2\right)^2\left(-(1+I)\left(\beta^2-\frac{\alpha^2}{3}\right)\alpha e^{L(I\beta-\alpha)}-\left(\frac{1}{3}+\frac{I}{3}\right)\beta(-3\alpha^2+\beta^2)e^{L((-2+I)\alpha+\beta)}+(-1+I)\left(\beta^2-\frac{\alpha^2}{3}\right)\alpha e^{-L(I\beta+\alpha)}\right)+\left(\frac{1}{3}-\frac{I}{3}\right)\beta e^{L(I\alpha+\beta)}(-3\alpha^2+\beta^2)}{-2\alpha^3\beta+2\alpha\beta^3}$$

$N1(4,4) = N1(3,3)$